
This is an electronic reprint of the original article.
This reprint may differ from the original in pagination and typographic detail.

Badar, Tabish; Backman, Juha; Tariq, Usama; Vísala, Arto

Nonlinear 6-DOF Dynamic Simulations for Center-Articulated Vehicles with combined CG

Published in:
IFAC-PapersOnLine

DOI:
[10.1016/j.ifacol.2022.07.589](https://doi.org/10.1016/j.ifacol.2022.07.589)

Published: 01/07/2022

Document Version
Publisher's PDF, also known as Version of record

Published under the following license:
CC BY-NC-ND

Please cite the original version:
Badar, T., Backman, J., Tariq, U., & Vísala, A. (2022). Nonlinear 6-DOF Dynamic Simulations for Center-Articulated Vehicles with combined CG. *IFAC-PapersOnLine*, 55(14), 95-100.
<https://doi.org/10.1016/j.ifacol.2022.07.589>

This material is protected by copyright and other intellectual property rights, and duplication or sale of all or part of any of the repository collections is not permitted, except that material may be duplicated by you for your research use or educational purposes in electronic or print form. You must obtain permission for any other use. Electronic or print copies may not be offered, whether for sale or otherwise to anyone who is not an authorised user.

Nonlinear 6-DOF Dynamic Simulations for Center-Articulated Vehicles with combined CG^{*}

Tabish Badar^{*} Juha Backman^{*,**} Usama Tariq^{*} Arto Visala^{*}

^{*} Department of Electrical Engineering and Automation, Aalto University, 02150 Espoo, Finland (e-mails: firstname.surname@aalto.fi)

^{**} Farming technologies, Natural Resources Institute Finland (Luke), Lönnrotinkatu 7, 50100 Mikkeli, Finland (e-mail: juha.backman@luke.fi)

Abstract: This study highlights a combined center of gravity (CG) approach to model the comprehensive dynamics of the ground vehicles with articulated steering using solely six degrees of freedom (6-DOF). It is the case with an articulated vehicle that its CG shifts laterally towards the center of rotation during a turn. Thus, the idea is to compute the combined CG position of the multi-body articulated vehicle, which leads to the correction of the moment arms and body inertias about the updated CG position in the dynamic equations. Hence, the body forces and moments are computed with respect to the corrected CG position. In addition, the paper illustrates mathematical modeling of the center-articulated steering mechanism for the ground vehicle while restricting its operation to the primary handling regime. Overall, the draft presents the design of a nonlinear 6-DOF simulation for a load-haul-dump (LHD) type of articulated vehicle with a traveling CG. The simulation data is presented from one simulation run, where the critical results are analyzed. The obtained results signify the simplicity in using a combined CG to represent the vehicle dynamics.

Copyright © 2022 The Authors. This is an open access article under the CC BY-NC-ND license (<https://creativecommons.org/licenses/by-nc-nd/4.0/>)

Keywords: Articulated steering, multi-body ground vehicles, nonlinear dynamic model, vehicle modeling and simulation, autonomous ground vehicles.

1. INTRODUCTION

At Aalto University, one of the research and development platforms for autonomous driving in uneven terrains is Rakkatec's unmanned ground vehicle as depicted in Figure 1. Rakka UGV is a load-haul-dump (LHD) type of articulated vehicle with center-articulated steering. The other machine of interest with articulated steering is Ponsse's Bison forwarder, which serves the purpose of transporting cut-to-length logs from forest stands to roadside. The main aspect of this study involves the demonstration of (semi-)autonomous driving in the uneven terrains using these vehicles. Therefore, it necessitates the development of a nonlinear simulation platform to test, for example, navigation and control methods for these vehicles. This study focuses on the development of a 6-DOF nonlinear dynamic model for the articulated vehicles using combined CG.

Altafini (1999) describes a load-haul-dump (LHD) type of articulated vehicle as a complex multi-body system that constitutes two bodies, namely front body and rear body, attached by a hitch point. The wheels attached to the front or rear bodies are non-steerable. In such vehicles, the joint provides steering to the connected bodies by varying the fluid pressures in the hydraulic actuators. The kinematic equations of motion of such vehicles are found either by considering a single-vehicle coordinate system as in Polotski and Hemami (1997) when the origin is attached to the articulation point, or by using two coordinate systems fixated to the centers of the front and rear axles (as discussed in Altafini (1999); Corke and Ridley (2001)). Polotski and Hemami (1997) further extended the kinematic model



Fig. 1. A photograph of the Rakkatec unmanned ground vehicle (Rakka-UGV). The vehicle can be seen maneuvering using center-articulated steering (courtesy: Rakkatec Ltd.).

to a kinetic one in Hemami and Polotski (1997), where the traction and articulation forces were further taken into account to derive, in particular, the equation for angular acceleration of the vehicle about the intersection point of the front and rear axles. Likewise, Lei et al. (2021) presented a planar model where the purpose is to perform the lateral stability analysis of the articulated vehicle with the focus on transverse swing characteristic of the vehicle. It, too, limits the study to flat and two-dimensional surfaces, which is certainly not the case in mining and forestry.

The limitation in describing an extensive dynamic model for the articulated vehicle is that it undergoes CG position variations during articulated steering. It is because of the lateral shift

^{*} The research is funded by the Technology Industries of Finland Centennial Foundation and Jane and Aatos Erkko Foundation.

of the articulated vehicle's CG along the radius of curvature while turning. Such a structural change impacts the fundamental assumption of the single rigid body with a fixed CG, which has been a norm to describe the dynamic equations of the conventional car-like vehicles so far. Eventually, it leads to the construction of complex nonlinear dynamic models with higher degrees of freedom, where the dynamic equations assume separate CGs fixed to the front and rear bodies of the articulated vehicle (see, for example, Li et al. (2013, 2014)). However, the dynamic models presented in Li et al. (2013, 2014) solely serve the purpose of simulating dynamics with no feasibility to extend these models to design control and estimation methods for articulated vehicles. Therefore, the motivation of this research is to extend the single rigid body assumption as presented in Hemami and Polotski (1997) to build a nonlinear 6-DOF simulation for the articulated vehicles.

The organization of the rest of the document is as follows. Brief details about a generalized 6-DOF (6 degrees of freedom) model of the vehicle used in the simulation are provided in Section 2. In Section 3, the problem addressed in this paper is formulated. Section 4 presents the impact of changes in joint inertia matrix and the vehicle CG position due to articulated steering on the resulting equations of motion (EOMs). In Section 5, we present the equations to compute sideslip angle using the velocities of each corner (strut-mounts) of the articulated vehicle. The CG position in the inertial frame is mentioned in Section 6. Next, the simulation results are discussed in Section 7. Finally, the conclusive remarks are mentioned in Section 8.

2. 6-DOF VEHICLE MODEL

Figure 2 illustrates a top schematic view of the vehicle under discussion. Point **P** is the location of the articulation joint with

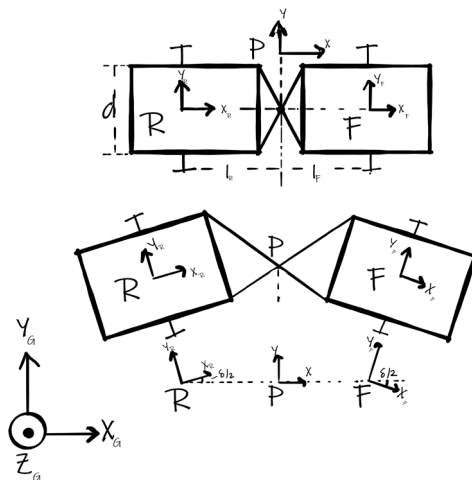


Fig. 2. Relations among different reference frames attached to the vehicle during articulation.

only one degree of freedom, the steering angle δ . Point **F** represents the point fixed to the center of front axle (CFA), whereas point **R** is attached to the center of rear axle (CRA). Further, we assume that a reference frame XYZ attached to **P**, a frame $X_F Y_F Z_F$ attached to CFA, and $X_R Y_R Z_R$ attached to CRA, respectively. Moreover, the coordinate system $X_G Y_G Z_G$ represents a global (inertial) frame of reference. The distance

from **P** to **F** is denoted by l_F , while the distance from **P** to **R** is represented by l_R . The total length of the vehicle is l , width d , and height h . During articulation, the frame of references attached to **P**, **F**, and **R** move with respect one another such that the frames $X_F Y_F Z_F$ and $X_R Y_R Z_R$ can be aligned to XYZ by angles $\delta/2$ and $-\delta/2$, respectively, provided $l_F = l_R$. Note that, the condition $l_F = l_R$, is true for the vehicle under discussion (Leander (2020)).

With articulated vehicles such as LHD and forwarders, it is the case that the wheels are modeled as a spring-damper system (see, for example, Li et al. (2013)). We consider three coordinate systems to express the comprehensive dynamics of the vehicle. The attitude and position of the body are measured in the global (inertial) frame of reference ($X_G Y_G Z_G$). The coordinate frame, $x'y'z'$, is attached to the tire ground contact patch. The subscript t is used to represent quantities in coordinate frame attached to the tire ground contact patch. In addition, we assume that a coordinate frame (xyz) is fixed to the vehicle's center of gravity (CG). The CG-fixed coordinate frame (xyz) is aligned with the motion of the combined center of the mass of the front and rear bodies. We will use subscript b to represent quantities in the vehicle body frame. The transformation from inertial coordinates ($X_G Y_G Z_G$) to body coordinates (xyz) follows the consecutive Euler angle rotations as defined in Etkin and Reid (1995).

The EOMs collected from Shim and Ghike (2007); Etkin and Reid (1995) are as follows:

$$\dot{X}_G = u \cos \theta \cos \psi + v(\cos \psi \sin \theta \sin \phi - \cos \phi \sin \psi) + w(\sin \phi \sin \psi + \cos \phi \cos \psi \sin \theta) \quad (1)$$

$$\dot{Y}_G = u \cos \theta \sin \psi + v(\cos \phi \cos \psi + \sin \theta \sin \phi \sin \psi) + w(\cos \phi \sin \theta \sin \psi - \cos \psi \sin \phi) \quad (2)$$

$$\dot{Z}_G = -u \sin \theta + v \cos \theta \sin \phi + w \cos \theta \cos \phi \quad (3)$$

$$\dot{u} = F_x/m + g \sin \theta - (qw - rv), \quad (4)$$

$$\dot{v} = F_y/m - g \sin \phi \cos \theta - (ru - pw), \quad (5)$$

$$\dot{w} = F_z/m - g \cos \phi \cos \theta - (pv - qu), \quad (6)$$

$$L = I_{xx} \dot{p} - I_{xy}(\dot{q} - rp) - (I_{yy} - I_{zz})qr - I_{yz}(q^2 - r^2) - I_{zx}(\dot{r} + pq), \quad (7)$$

$$M = I_{yy} \dot{q} - I_{xy}(\dot{p} + qr) - (I_{zz} - I_{xx})rp - I_{zx}(r^2 - p^2) - I_{yz}(\dot{r} - pq), \quad (8)$$

$$N = I_{zz} \dot{r} - I_{xy}(p^2 - q^2) - (I_{xx} - I_{yy})pq - I_{yz}(\dot{q} + rp) - I_{zx}(\dot{p} - qr), \quad (9)$$

$$\dot{\psi} = q \sin \phi \sec \theta + r \cos \phi \sec \theta, \quad (10)$$

$$\dot{\theta} = q \cos \phi - r \sin \phi, \quad (11)$$

$$\dot{\phi} = \dot{\psi} \sin \theta + p. \quad (12)$$

The position coordinates (X_G, Y_G, Z_G) represent the position of vehicle's CG in global frame of reference. The body velocities, i.e. the linear velocities of the vehicle CG are defined as longitudinal (forward) velocity (u), lateral (left-side) velocity (v), and up velocity (w). The state vector contains roll rate (p), pitch rate (q), and yaw rate (r) which are the angular velocities of the vehicle frame about CG. Finally, the state vector constitutes Euler angles, that are roll angle (ϕ – positive right-side down), pitch angle (θ – positive front-side down), and yaw angle (ψ – positive counterclockwise). Thus, the state vector is defined as $\mathbf{X} = \{X_G, Y_G, Z_G, u, v, w, p, q, r, \psi, \theta, \phi\}$. F_x , F_y , and F_z are forces experienced by the vehicle body along x , y , and z axes, respectively. L , M , and N are the rolling,

pitching and yawing moments of the vehicle body, respectively. The forces and moments include those transmitted to the sprung mass via tires – modeled as spring-damper systems – at each corner of the vehicle (Li et al. (2013)). m is the body mass of the vehicle. g is the acceleration due to gravity. I_{xx} , I_{yy} , and I_{zz} are the moments of inertia, whereas I_{xy} , I_{yz} , and I_{zx} are the products of inertia of the vehicle body around its CG.

It is crucial to highlight here that the the body inertia values vary as the CG shifts since assumption that the CG remains fixed to some reference point of the vehicle (such as \mathbf{P}) is not valid for the articulated vehicles. This point is further highlighted in the next section.

3. PROBLEM FORMULATION

First, let us define the inertia matrix of the vehicle assuming a single rigid body as:

$$\mathbf{I}_B = \begin{bmatrix} I_{xx} & -I_{xy} & I_{xz} \\ -I_{yx} & I_{yy} & -I_{yz} \\ -I_{zx} & -I_{zy} & I_{zz} \end{bmatrix} \quad (13)$$

where

$$I_{xx} = \int (y^2 + z^2) dm;$$

$$I_{yy} = \int (x^2 + z^2) dm;$$

$$I_{zz} = \int (x^2 + y^2) dm$$

are the moments of inertia of the rigid body around its CG along x , y , and z axes, respectively. Moreover, the off-diagonal elements are the products of inertia of the vehicle defined as:

$$I_{xy} = \int xy dm; \quad I_{zx} = \int xz dm; \quad I_{yz} = \int yz dm$$

where

$$I_{xy} = I_{yx}; \quad I_{zx} = I_{xz}; \quad I_{yz} = I_{zy}.$$

Equations (7–9) can be simplified further if we assume that a plane of symmetry exists for the vehicle. Commonly, xz -plane is assumed to be the plane of symmetry for the vehicle. In Etkin and Reid (1995), it is assumed for the air vehicles, however, we extend the same assumptions to the case of ground vehicles. Consequently, this leads to simplification where

$$I_{xy} = I_{yz} = 0.$$

Furthermore, the only remaining off-diagonal term I_{xz} can be eliminated if the direction of body axes coincide with the principle axes (direction of motion) of the vehicle as discussed in Shim and Ghike (2007). Under such assumptions, \mathbf{I}_B becomes a diagonal matrix.

As mentioned above, this is generally not the case with ground vehicles with articulated steering due to the relative motion of front and rear bodies. Moreover, the net inertia matrix \mathbf{I}_B of the articulated vehicle may alter when the mass of the front body or the rear body changes during loading. In addition, the dimensions of the front and rear body is not exactly the same in almost every situation. Next, we present an elementary solution to this problem in where the aim is to preserve the conventional form of the EOMs, as mentioned in Etkin and Reid (1995); Shim and Ghike (2007).

4. CG CORRECTED MOMENT EQUATIONS

The procedure is detailed as follows:

- (1) Firstly, the origin $(0, 0, 0)$ of the vehicle is assumed to be fixed at the point of articulation \mathbf{P} .
- (2) Further, we assume that the front and rear bodies are cuboids with homogeneous mass distribution with individual inertia matrices, denoted by $\mathbf{I}_{B,F}$ and $\mathbf{I}_{B,R}$, respectively. These inertia matrices are considered diagonal matrices for the reasons discussed earlier.
- (3) The position vectors of the strut mounting points ($\tilde{\mathbf{p}}_{kl}$) and CG locations of the front ($\tilde{\mathbf{p}}_{CG,F}$) and rear ($\tilde{\mathbf{p}}_{CG,R}$) bodies are defined about the origin of the vehicle. Thus, each position vector rotates about the origin during articulated steering.
- (4) Thus, during articulated steering the combined CG position of the vehicle \mathbf{p}_{CG} is given as

$$\mathbf{p}_{CG} = \frac{m_F \mathbf{R}_z(\delta/2) \tilde{\mathbf{p}}_{CG,F} + m_R \mathbf{R}_z(-\delta/2) \tilde{\mathbf{p}}_{CG,R}}{m_R + m_F} \quad (14)$$

where $\mathbf{R}_z(\cdot)$ is the rotation matrix (see, Appendix A for its definition), and m_F and m_R denote the mass of front and rear bodies, respectively. Note that, we are assuming the articulation joint to have only one degree of freedom, i.e., the joint can only rotate about z -axis.

- (5) Further, we correct the displacement of the CG positions of the front and rear bodies for the updated vehicle CG position as

$$\mathbf{p}_{CG,F} = \mathbf{R}_z(\delta/2) \tilde{\mathbf{p}}_{CG,F} - \mathbf{p}_{CG}; \quad (15)$$

and

$$\mathbf{p}_{CG,R} = \mathbf{R}_z(-\delta/2) \tilde{\mathbf{p}}_{CG,R} - \mathbf{p}_{CG}. \quad (16)$$

- (6) We compute the net inertia tensors \mathbf{I}_B by combining two cuboids after rotating constituent parts by articulation angle and applying parallel axes theorem for the displacements of CG positions $\mathbf{p}_{CG,F}$ and $\mathbf{p}_{CG,R}$. Thus, we get

$$\mathbf{I}_B = \mathbf{R}_z(\delta/2) \mathbf{I}_{B,F} \mathbf{R}_z(\delta/2)^T + \mathbf{R}_z(-\delta/2) \mathbf{I}_{B,R} \mathbf{R}_z(-\delta/2)^T + \sum_i m_i ((\mathbf{p}_{CG,i}^T \mathbf{p}_{CG,i}) \mathbf{E}_3 - (\mathbf{p}_{CG,i} \mathbf{p}_{CG,i}^T)), \quad (17)$$

where $i = \{F, R\}$ represent the front and rear bodies, \mathbf{E}_3 is a 3x3 identity matrix, and superscript T shows the vector (or matrix) transpose.

- (7) Subsequently, the new moment arms and inertia values are used to compute angular accelerations from equations 7–9.

It is straightforward to notice that besides the diagonal terms of \mathbf{I}_B , the only nonzero term would be I_{xy} due to uneven mass distributions, for example, due to cargo loading to the rear body. However, I_{yz} and I_{xz} terms remain zero because of symmetric dimensions of the cuboids. This leads to re-writing equations (7–9) for body rates as

$$\begin{bmatrix} \dot{p} \\ \dot{q} \\ \dot{r} \end{bmatrix} = \begin{bmatrix} I_{xx} & -I_{xy} & 0 \\ -I_{yx} & I_{yy} & 0 \\ 0 & 0 & I_{zz} \end{bmatrix}^{-1} \begin{bmatrix} L_p \\ M_q \\ N_r \end{bmatrix} \quad (18)$$

where

$$L_p = L - I_{xy}rp + (I_{yy} - I_{zz})qr, \quad (19)$$

$$M_q = M + I_{xy}qr + (I_{zz} - I_{xx})rp, \quad (20)$$

$$N_r = N + I_{xy}(p^2 - q^2) + (I_{xx} - I_{yy})pq. \quad (21)$$

It is crucial to mention here that the moment arms (or lever arms) used to compute the body moments L , M , and N due to tire forces have to be corrected for \mathbf{p}_{CG} . It is achieved by

correcting the position vectors associated with each strut-mount (corner) of the vehicle with respect to corrected CG position as

$$\mathbf{p}_{kl} = \mathbf{R}_z(\delta_{kl})\tilde{\mathbf{p}}_{kl} - \mathbf{p}_{CG}, \quad (22)$$

where the subscript (kl) represents left front (lF), right front (rF), left rear (lR), and right rear (rR) tires and strut-mounts. δ_{kl} denotes the steering angle for each tire location, such that for front tires we have

$$\delta_{kF} = \delta/2; \quad (23)$$

whereas for rear wheels, we have

$$\delta_{kR} = -\delta/2, \quad (24)$$

provided $l_F = l_R$.

Next, we move on to discuss the computation of tire forces assuming the vehicle operates in the primary handling regime.

5. CG CORRECTED TIRE FORCES

In this study, each tire only introduces a central force component (F_s) and a drag force components (F_d) to the 6-DOF model by resolving the tire forces into $x'y'z'$ coordinate by the steering angle (Dixon (1996)). Thus, additional degree of freedom due to spinning of each wheel is not considered in the simulations. Furthermore, to model tire forces in the non-linear 6-DOF simulations, we restrict ourselves to the primary handling regime. Dixon (1988) noted four types of handling regions for a ground vehicle (either car or truck) by describing the variation of the steering angle δ with the lateral acceleration a_c . The range of a_c in the primary handling regime goes up to 3 m/s^2 for cars and 1 m/s^2 for trucks. For Rakka UGV to operate in primary handling regime, it implies that for the commanded steering angle and nominal speed of the vehicle the condition $a_c < 1 m/s^2$ is always satisfied.

In such a case, the lateral tire force $F_{y_{kl}}$ is related to the sideslip angle α_{kl} as

$$F_{y_{kl}} = -C_{\alpha,kl}\alpha_{kl}, \quad (25)$$

where $C_{\alpha,kl}$ is the cornering stiffness of kl th tire. In the coordinate frame ($x'y'z'$) fixed to the tire ground contact patch, the lateral slip angle is given as (Shim and Ghike (2007))

$$\alpha_{kl} = \tan^{-1}\left(\frac{v_{t,kl}}{u_{t,kl}}\right) - \delta_{kl}, \quad (26)$$

where $u_{t,kl}$, $v_{t,kl}$, and $w_{t,kl}$ are the longitudinal, lateral, and vertical velocities at the tire-ground contact point in the $x'y'z'$ coordinate frame. These velocities can be obtained by first transforming the CG velocities to the velocities of strut-mount points expressed in the body-fixed coordinate frame as

$$\begin{bmatrix} u_{b,kl} \\ v_{b,kl} \\ w_{b,kl} \end{bmatrix} = \begin{bmatrix} u \\ v \\ w \end{bmatrix} - \dot{\mathbf{R}}_z(\delta_{kl}, \dot{\delta}_{kl})\tilde{\mathbf{p}}_{kl} + \left(\dot{\mathbf{R}}_x(0, p) + \dot{\mathbf{R}}_y(0, q) + \dot{\mathbf{R}}_z(0, r)\right)\mathbf{p}_{kl}, \quad (27)$$

where \mathbf{p}_{kl} is CG corrected position of each strut-mounting point, $\tilde{\mathbf{p}}_{kl}$ is strut-mount position with respect to point \mathbf{P} . Moreover, $\dot{\mathbf{R}}_x(\cdot, \cdot)$, $\dot{\mathbf{R}}_y(\cdot, \cdot)$, and $\dot{\mathbf{R}}_z(\cdot, \cdot)$ are the time derivatives of the respective rotation matrices. Subsequently, the velocities of the strut mounting points in the CG-fixed coordinate frame are transformed to the velocities in the $x'y'z'$ coordinate frame as

$$\begin{bmatrix} u_{t,kl} \\ v_{t,kl} \\ w_{t,kl} \end{bmatrix} = \mathbf{R}_y(\theta)\mathbf{R}_x(\phi) \begin{bmatrix} u_{b,kl} \\ v_{b,kl} \\ w_{b,kl} \end{bmatrix}. \quad (28)$$

In addition, we model the longitudinal force on the kl th tire as

$$F_{x_{kl}} = \mu F_{z_{kl}}, \quad (29)$$

where μ is the friction coefficient. Finally, the wheel forces in body frame are obtained by transforming the tire forces to the strut-aligned (or, vehicle motion aligned) forces. Such transformation is obtained by

$$\begin{bmatrix} F_{x_{b,kl}} \\ F_{y_{b,kl}} \\ F_{z_{b,kl}} \end{bmatrix} = \mathbf{R}_x(-\phi)\mathbf{R}_y(-\theta) \begin{bmatrix} F_{x_{t,kl}} \\ F_{y_{t,kl}} \\ F_{z_{t,kl}} \end{bmatrix}, \quad (30)$$

where we obtain the tire forces in wheel-centered coordinate frame by resolving the longitudinal ($F_{x_{kl}}$) and lateral ($F_{y_{kl}}$) tire forces as

$$\begin{bmatrix} F_{x_{t,kl}} \\ F_{y_{t,kl}} \\ F_{z_{t,kl}} \end{bmatrix} = \mathbf{R}_z(\delta_{kl}) \begin{bmatrix} F_{x_{kl}} \\ F_{y_{kl}} \\ F_{z_{kl}} \end{bmatrix}. \quad (31)$$

It is crucial to highlight here that the change in CG manifests itself in the body acceleration equations as additional velocity components introduced by $\dot{\mathbf{R}}_z(\delta_{kl}, \dot{\delta}_{kl})\mathbf{p}_{kl}$ in the velocities of each corner of the vehicle. The CG-shifted velocities of each corner $u_{b,kl}$, $v_{b,kl}$, and $w_{b,kl}$ are used to compute sideslip angles α_{kl} . This ultimately leads to the computation of the body forces $F_{x_{b,kl}}$, $F_{y_{b,kl}}$, and $F_{z_{b,kl}}$ with respect to corrected CG. Subsequently, these body forces are used to update body acceleration using equations (4–6) corresponding to new CG location (\mathbf{p}_{CG}).

6. CG POSITION IN INERTIAL FRAME

Exclusively, there remains a requirement to modify equations (1–3) to obtain the corrected CG positions in the inertial (global) frame of reference. Using vector-matrix notations for convenience, it is solely achievable by re-writing equations (1–3) as

$$\begin{bmatrix} \dot{X}_G \\ \dot{Y}_G \\ \dot{Z}_G \end{bmatrix} = \mathbf{C}_b^G \left(\begin{bmatrix} u \\ v \\ w \end{bmatrix} + \dot{\mathbf{p}}_{CG} \right), \quad (32)$$

where

$$\mathbf{C}_b^G = \mathbf{R}_z(\psi)\mathbf{R}_y(\theta)\mathbf{R}_x(\phi) \quad (33)$$

is the transformation matrix to convert body coordinates to global coordinates, and $\dot{\mathbf{p}}_{CG}$ is obtained by taking derivative of equation (14) as

$$\dot{\mathbf{p}}_{CG} = \frac{m_F \dot{\mathbf{R}}_z(\delta/2, \dot{\delta}/2)\tilde{\mathbf{p}}_{CG,F} + m_R \dot{\mathbf{R}}_z(-\delta/2, -\dot{\delta}/2)\tilde{\mathbf{p}}_{CG,R}}{m_R + m_F} \quad (34)$$

provided masses m_F and m_R do not change during vehicle operation.

7. SIMULATION RESULTS

In this section, we discuss the results obtained from a simulation run. The important vehicle parameters used in the simulation are mentioned in Table 1. Figure 3 illustrates the open loop responses corresponding to forward acceleration $a_x = \dot{u}$, ground speed $V_g = \sqrt{u^2 + v^2}$, steering angle δ_d , and yaw rate r of Rakka UGV. Here, the actual inputs to the dynamic model are the acceleration a_{xc} and rate of change steering command $d(\delta_c)/dt$ commands. The steering angle command δ_c is obtained by integration of $d(\delta_c)/dt$ command. Likewise, the speed command V_c is obtained by integrating a_{xc} while the

Table 1. Vehicle Parameters

Quantity	Specification
Type	Rakka UGV
Mass (Self)	3000 kg
Gross Weight	6000 kg
Length of the Vehicle	4.6 m
Width	2.1 m
Height	1.1 m
Distance from front axle to joint	0.95 m
Distance from rear axle to joint	0.95 m
Distance between axles	2 m
Minimum Turning Radius (r_c)	2.3 m
Rated Speed (V_c)	0.44 m/s
Maximum Steering Angle (δ_c)	$\pm 33^\circ$
Maximum Steering Rate ($d(\delta_c)/dt$)	$\pm 17^\circ/s$

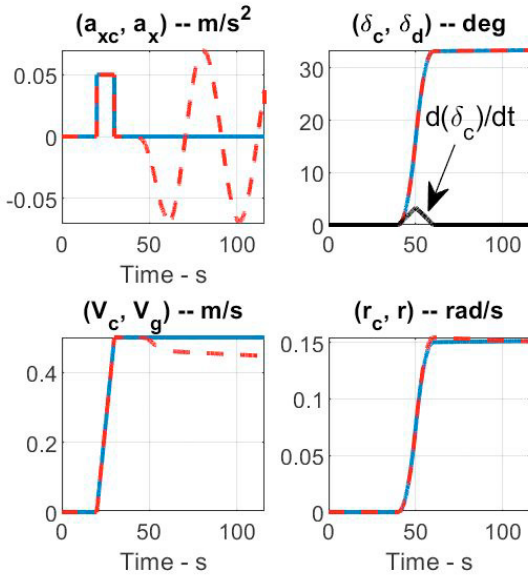


Fig. 3. The inputs forward acceleration command a_{xc} , speed command V_c , steering rate command $d(\delta_c)/dt$, and yaw rate command r_c are shown in blue. The output responses of Rakka UGV (a_x , V_g , δ_d , and r) are shown in dashed red lines.

commanded yaw rate r_c is computed by V_c/r_c . It is important to mention here that for the Rakka UGV a_{xc} and $d(\delta_c)/dt$ commands are adjusted such that the maximum speed of the vehicle does not exceed 0.5 m/s, whereas the maximum steering angle and steering rate for Rakkatec platform are always within prescribed limits of $\pm 33^\circ$ and $\pm 17^\circ/s$, respectively. This is to ensure that the condition $a_c < 1 \text{ m/s}^2$ is always met.

In Figure 4, the (X, Y) trajectory shown in blue represents the path traveled by the CG as computed by the dynamic model, whereas the trajectory shown in red depicts the path traversed by the articulation point P in the inertial frame. Notice that the tighter turn of the CG in Figure 4 is reflected by lower radius of curvature in comparison to the articulation point P . It highlights that the CG shift towards instantaneous center of rotation (ICR) during turn that eventually results in a smaller radius of curvature.

Figure 5 shows the roll profile of the vehicle. During articulated turn, the CG shifts to the left of point P resulting in a negative roll angle, indicating the right-side of the vehicle moving slightly upwards as CG shifts to the left. Figure 6 illustrates the

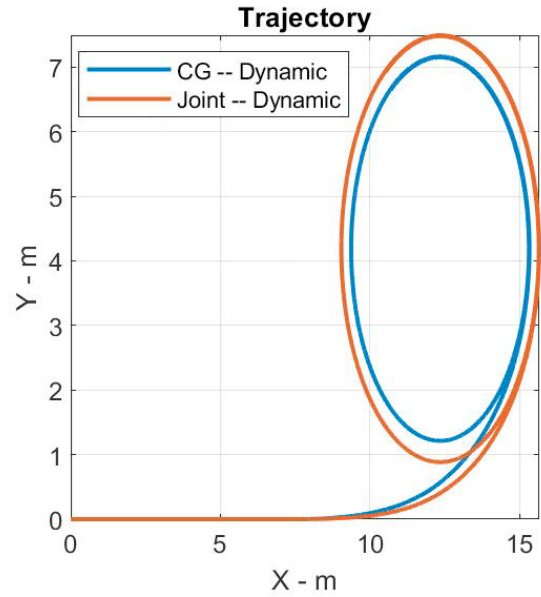


Fig. 4. (X, Y) -path simulation results traversed by the CG (shown in blue) and the point of articulation P (shown in red) of Rakka UGV.

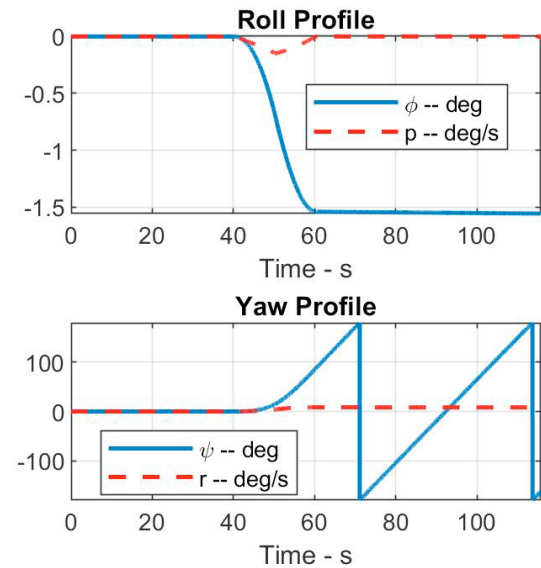


Fig. 5. **Top:** Roll angle profile of the vehicle is shown. **Bottom:** Profile corresponding to evolution of yaw angle ψ and yaw rate r is shown.

change in the height of the CG due to spring compression from initial height of 0m. It also depicts the change in pitch angle as the vehicle starts accelerating forward. Note that, here negative pitch implies front-side down of the vehicle. One critical observation to made from Figure 6 is the nonzero pitch rate q after time $t = 60$ sec. Notice that the pitch rate is in the body frame, however the pitch angle is in an inertial frame. Since the roll angle is nonzero after time $t = 60$ sec, the yaw turning is seen in pitch rate even though the pitch angle does not change.

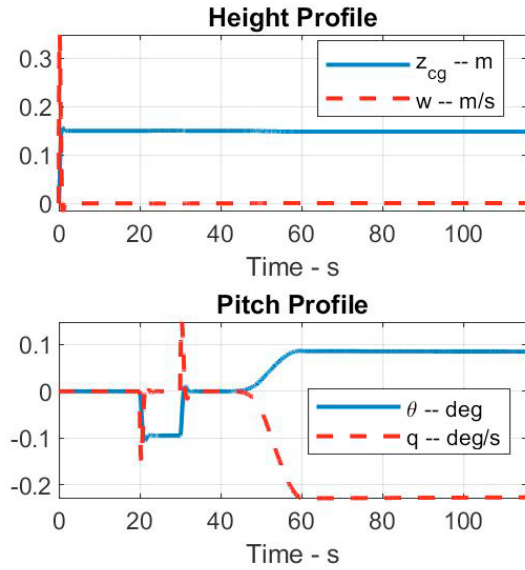


Fig. 6. **Top:** z_{cg} corresponds to height of CG in the inertial frame. w represents the up-velocity of the CG. **Bottom:** Evolution of pitch angle θ and pitch rate q in the simulation.

8. CONCLUSIONS AND FUTURE WORK

This paper highlights the efficacy of using a combined CG to simulate 6-DOF dynamic model of the ground vehicles with center-articulated steering. At first, it is necessary to compute the CG and joint inertia matrix of the vehicle during articulated steering. The lever arms are shifted as seen from the new CG position at each simulation time step. Accordingly, the equations for body torques (moments), forces, and inertial positions of the vehicle with respect to corrected CG is computed. A realistic scenario is simulated to study the turning characteristics of an articulated vehicle of choice at the rated speed and maximum steering angle. The analysis of the simulation results shows that the dynamic model predicts the cornering behavior realistically.

These results are crucial in, for example, designing model-based speed and steering controllers for the articulated vehicles. The simulation platform will provide a functional basis for furthering the mathematical model for articulated forest machines considering uneven terrains.

ACKNOWLEDGEMENTS

The authors acknowledge the role of the Department of Electrical Engineering and Automation at Aalto University to make this research possible. Special thanks to the Technology Industries of Finland Centennial Foundation and Jane and Aatos Erkkö Foundation for providing necessary funding for the AUTOLOGGER project under The Future Makers program.

REFERENCES

- Altafini, C. (1999). A path-tracking criterion for an lhd articulated vehicle. *The International Journal of Robotics Research*, 18(5), 435–441.
- Corke, P. and Ridley, P. (2001). Steering kinematics for a center-articulated mobile robot. *IEEE Transactions on Robotics and Automation*, 17(2), 215–218.

- Dixon, J.C. (1988). Linear and non-linear steady state vehicle handling. *Proceedings of the Institution of Mechanical Engineers, Part D: Transport Engineering*, 202(3), 173–186.
- Dixon, J.C. (1996). *Tires, Suspension and Handling*. SAE International, USA, second edition.
- Etkin, B. and Reid, L.D. (1995). *Dynamics of Flight: Stability and Control*. John Wiley and Sons, USA, third edition.
- Hemami, A. and Polotski, V. (1997). Dynamics of a dual-unit articulated vehicle for path tracking control problem formulation. In *Proceedings of the 1997 IEEE International Conference on Control Applications*, 173–176.
- Leander, P. (2020). *Local Path Planning and Tracking Algorithm for a Center-Articulated Vehicle*. Master's thesis, Aalto University. School of Electrical Engineering.
- Lei, T., Wang, J., and Yao, Z. (2021). Modelling and stability analysis of articulated vehicles. *Applied Sciences*, 11(8).
- Li, X., Wang, G., Yao, Z., and Qu, J. (2013). Dynamic model and validation of an articulated steering wheel loader on slopes and over obstacles. *Vehicle System Dynamics*, 51(9), 1305–1323.
- Li, X., Wang, G., Yao, Z., and Yang, Y. (2014). Research on lateral stability and rollover mechanism of articulated wheel loader. *Mathematical and Computer Modelling of Dynamical Systems*, 20(3), 248–263.
- Polotski, V. and Hemami, A. (1997). Control of articulated vehicle for mining applications: modeling and laboratory experiments. In *Proceedings of the 1997 IEEE International Conference on Control Applications*, 318–323.
- Shim, T. and Ghike, C. (2007). Understanding the limitations of different vehicle models for roll dynamics studies. *Vehicle System Dynamics*, 45(3), 191–216.

Appendix A. ROTATION MATRICES

For convenience of expression, the rotation matrices about x , y , and z -axes are defined as follows:

$$\mathbf{R}_x(\phi) = \begin{bmatrix} 1 & 0 & 0 \\ 0 & \cos \phi & -\sin \phi \\ 0 & \sin \phi & \cos \phi \end{bmatrix}, \quad (\text{A.1})$$

$$\mathbf{R}_y(\theta) = \begin{bmatrix} \cos \theta & 0 & \sin \theta \\ 0 & 1 & 0 \\ -\sin \theta & 0 & \cos \theta \end{bmatrix}, \quad (\text{A.2})$$

with

$$\mathbf{R}_z(\psi) = \begin{bmatrix} \cos \psi & -\sin \psi & 0 \\ \sin \psi & \cos \psi & 0 \\ 0 & 0 & 1 \end{bmatrix}. \quad (\text{A.3})$$

The time derivatives of the rotation matrices are given as follows:

$$\dot{\mathbf{R}}_x(\phi, \dot{\phi}) = \begin{bmatrix} 0 & 0 & 0 \\ 0 & -\sin \phi & -\cos \phi \\ 0 & \cos \phi & -\sin \phi \end{bmatrix} \dot{\phi}, \quad (\text{A.4})$$

$$\dot{\mathbf{R}}_y(\theta, \dot{\theta}) = \begin{bmatrix} -\sin \theta & 0 & \cos \theta \\ 0 & 1 & 0 \\ -\cos \theta & 0 & -\sin \theta \end{bmatrix} \dot{\theta}, \quad (\text{A.5})$$

and

$$\dot{\mathbf{R}}_z(\psi, \dot{\psi}) = \begin{bmatrix} -\sin \psi & -\cos \psi & 0 \\ \cos \psi & -\sin \psi & 0 \\ 0 & 0 & 1 \end{bmatrix} \dot{\psi}. \quad (\text{A.6})$$